HAL
open science

# Development of microdevices for the in-plane thermoelectric characterization of deposited films

David Osenberg, Cristina Manzano, Marisol Martín-González, Nicolas Stein, Mélanie de Vos, Stefano Mischler, David Lacroix, Gilles Pernot, Laetitia Philippe

## To cite this version:

David Osenberg, Cristina Manzano, Marisol Martín-González, Nicolas Stein, Mélanie de Vos, et al.. Development of microdevices for the in-plane thermoelectric characterization of deposited films. Journal of Materials Research and Technology, 2021, 15, pp.1190-1200. 10.1016/j.jmrt.2021.08.109 . hal-03342438

**HAL Id: hal-03342438**

**https://hal.univ-lorraine.fr/hal-03342438v1**

Submitted on 15 Apr 2024

**HAL** is a multi-disciplinary open access archive for the deposit and dissemination of scientific research documents, whether they are published or not. The documents may come from teaching and research institutions in France or abroad, or from public or private research centers.

L'archive ouverte pluridisciplinaire **HAL**, est destinée au dépôt et à la diffusion de documents scientifiques de niveau recherche, publiés ou non, émanant des établissements d'enseignement et de recherche français ou étrangers, des laboratoires publics ou privés.

JOURNAL OF MATERIALS RESEARCH AND TECHNOLOGY 2021;15:1190–1200

Available online at www.sciencedirect.com

jmr&t
Journal of Materials Research and Technology

journal homepage: www.elsevier.com/locate/jmrt

Original Article

# Development of microdevices for the in-plane thermoelectric characterization of deposited films

David Osenberg [a,b,*], Cristina V. Manzano [c], Marisol Martín-González [c], Nicolas Stein [d], Mélanie De Vos [d], Stefano Mischler [b], David Lacroix [e], Gilles Pernot [e], Laetitia Philippe [a,1]

[a] Laboratory for Mechanics of Materials and Nanostructures, Empa (Swiss Federal Laboratories for Materials Testing and Research), Thun, Switzerland
[b] Tribology and Interfacial Chemistry Group, Institute of Materials, École Polytechnique Fédérale de Lausanne, Lausanne, Switzerland
[c] Instituto de Micro y Nanotecnología, IMN-CNM, CSIC (CEI UAM+CSIC), Madrid, Spain
[d] Université de Lorraine, CNRS, IJL, F-57000 Metz, France
[e] Université de Lorraine, CNRS, LEMTA, F-54000 Nancy, France

ARTICLE INFO

*Article history:*
Received 7 June 2021
Accepted 18 August 2021
Available online 27 August 2021

*Keywords:*
Thermoelectric characterization
Thermal transport
MEMS
Electrodeposition

ABSTRACT

Measuring the thermoelectric transport properties of a material is a prerequisite to determining its usefulness for application in waste heat recovery or cooling and the basis for devising improvement strategies. While well-established characterization methods exist for bulk samples, characterization of microscale samples remains challenging. This usually results in incomplete characterization such as restriction to study of the thermal transport properties, which can be misleading. While elaborate microdevices for complete thermoelectric characterization have been fabricated, a demanding transfer of the samples onto these devices is generally required and establishing sufficient electrical contact can be challenging in this case. Therefore a complete and transfer free in-plane characterization method for samples obtained by deposition processes was developed. The approach is based on expanding a well-established self-heating technique for the measurement of electrical and thermal conductivity to allow, in addition, for the measurement of the Seebeck coefficient. The fabrication exclusively involves photolithography and wet etching, with no need for other steps like electron-beam lithography and a lift-off process. The accuracy of the method is verified by numerical studies closely mimicking the actual measurement process, comparison to measurements on simultaneously deposited reference samples and results from literature.

© 2021 The Authors. Published by Elsevier B.V. This is an open access article under the CC BY license (http://creativecommons.org/licenses/by/4.0/).

* Corresponding author.
E-mail address: David.Osenberg@empa.ch (D. Osenberg).
[1] Present address: Research and Development, Rolex, Berne, Switzerland.

https://doi.org/10.1016/j.jmrt.2021.08.109
2238-7854/© 2021 The Authors. Published by Elsevier B.V. This is an open access article under the CC BY license (http://creativecommons.org/licenses/by/4.0/).

## 1. Introduction

It has been shown that the maximum thermoelectric conversion efficiency depends only on the temperature of the reservoirs and the dimensionless figure of merit, $zT_m = \frac{S^2\sigma}{\kappa}T_m$, where $T_m$ is the average temperature. This explains why research in thermoelectric conversion revolves around the problem of enhancing the thermoelectric figure of merit. Different kinds of approaches have been taken to enhance the figure of merit [1,2]. Most of the recent breakthroughs in enhancing the figure of merit can be attributed to nanostructuring [3]. In many cases obtaining bulk thermoelectric materials that can undergo conventional thermoelectric characterization methods by nanostructuring is not feasible. This particularly applies to deposition based fabrication methods, namely electrochemical [4,5] and physical [6–8] or chemical [9] vapor deposition. Typically these processes are limited to the deposition of films on the order of micrometers, which highlights the importance of measuring the thermoelectric properties of films. For microscale samples different characterization methods have been developed. Few allow the measurement of all required material properties on the same sample and even fewer along the same orientation. The latter can be important as many thermoelectric materials exhibit anisotropy [10]. Samples obtained by deposition processes typically have low aspect ratios. Therefore the term "cross-plane" is used to refer to measurements in the growth direction, while "in-plane" is used to refer to measurements orthogonal to the growth direction. The thermal conductivity is usually measured cross-plane by approaches such as the $3\omega$-, time-domain thermoreflectance or photoacoustic methods [11–14], since the supporting substrate acts as a heat sink. The electrical conductivity is advantageously measured in-plane. In case of cross-plane measurements spreading resistance within the sample and the substrate can be significant [15].

In case of exclusively in-plane measurements it is usually necessary to release samples from the substrate, as the substrate can thermally short circuit the samples. In 2001 a suspended microbridge device for the measurement of the thermoelectric properties of carbon nanotubes was designed by Li Shi [16]. Since then devices of this kind have been used for thermoelectric characterization of diverse materials [17–19]. They can be considered one of the most accurate, precise and comprehensive characterization methods. The measurements are conducted in vacuum to avoid heat transfer by convection and the microscale sample length together with the use of a radiation shield ensures that radiative heat transfer can be ignored. The main disadvantage of these devices is the complexity of the fabrication process, generally requiring at least two lithography steps, namely a lift-off process for the deposition of resistance thermometers, microheaters and electrodes and a second step for the patterning of the dielectric layer. Moreover the transfer of the microscale samples onto the measurement device is required, which typically involves subsequent patterning of the sample and an other metallization step or annealing to ensure good electrical contact. The latter can be vital as often a pseudo 4-probe measurement is employed. A method based on a similar micro-bridge device but specifically designed for the in-plane characterization of electrodeposited samples was recently proposed [20]. This approach is based on patterning of resistance thermometers and heaters and backside etching to suspend the sample. However, as the authors state, it is limited to the characterization of sufficiently thermally conductive samples, as the ratio of heat conducted through the resistance thermometers and heat conducted through the sample is assumed to be negligible. In case of 6 μm thick samples of thermal conductivity 2 $Wm^{-1}K^{-1}$, typical for $Bi_2Te_3$ at room temperature, the measured thermal conductivity severely exceeds the correct value (by 475%, supporting information of [20]).

Therefore in this study microdevices designed for the in-plane thermoelectric characterization of samples obtained by deposition processes, electroplating in particular, were investigated. The thermal conductivity is measured by a self-heating approach introduced in 2009 [21,22], while an additional electrode is used for the measurement of the thermopower. Thus all the three thermoelectric parameters are determined and the advantages of this method are the comparatively simple fabrication process, avoiding sample transfer and its negative consequences and accurate measurements over a wide range of thermoelectric sample properties. The developed method is validated by numerical modelling, comparison to results from literature and to measurements on reference samples.

## 2. Methods

### 2.1. *Device design and measurement method*

The idea of the approach is to expand the self-heating method for measuring not only the thermal and electrical conductance but also the thermopower of suspended samples. This method, briefly described above, exploits the temperature dependence of the sample's electrical resistance. The measurement of thermopower requires generating temperature differences between electrodes contacting the sample. As depicted in Fig. 1a the device consists of a suspended electrodeposited sample supported at its center by an electrode, consisting of gold underlying the electrodeposited film. The electrode itself is supported by a film of silicon oxide (about 1 μm thick) and silicon. Anisotropic silicon etching is applied to fabricate this partially suspended and supported structure. Since the central electrode is supported by silicon, acting as a heatsink, even application of currents through the suspended samples that cause its average temperature to increase significantly, has no significant effect on the temperature of the supported central segment. By applying currents at least two orders of magnitude higher than the sample currents through the central electrode, referred to as heating current in the following, temperature excursions in the central segment can be generated. Therefore by design of the device the temperature of the central segment can be controlled by the current through the central electrode, irrespective of the sample current. So in a first measurement, applying no heating current to the central electrode, the electrical and thermal conductance are determined as follows.

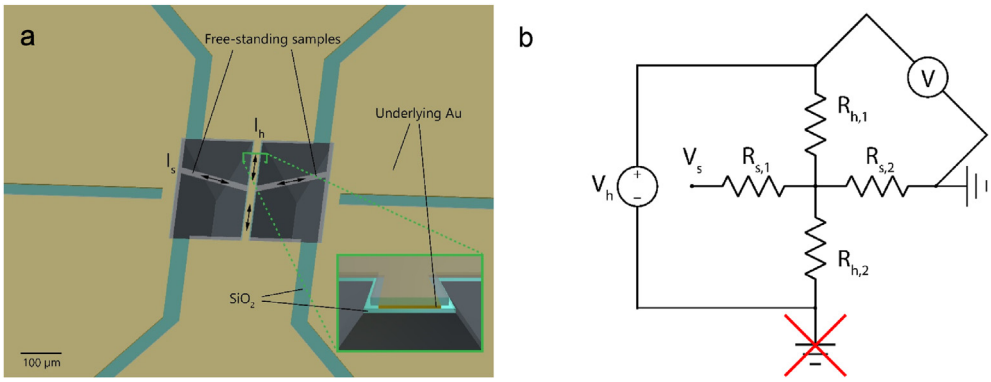


**Fig. 1 – Schematic of the device for the in-plane measurement of thermoelectric properties (a). The inset is a close-up of a cross-section view of the supported central electrode. (b) Equivalent circuit of the device modelling the electrical properties including the voltage sources. The heating current source is assumed to be isolated from ground.**

The electrical conductance is determined by measurement of the differential resistance, i.e. the slope of V-I curves for small sample current excursions to avoid Joule heating. The current range is adjusted based on the sample properties, but generally does not exceed 100 µA.

The thermal conductance is obtained by measuring the static electrical resistance of the sample as a function of the power $P$ dissipated in the sample (the product of the voltage and the applied dc current). In this case an order of magnitude greater sample currents are applied. In a sample of uniform composition and cross section Joule heating leads to a parabolic temperature profile if conduction is the only mode of heat transfer. If the ends of the sample are connected to a heatsink one can show that $\overline{\Delta T_s} = \frac{P}{12K_s}$, where $K_s$ denotes the thermal conductance of the sample [21] and $\overline{\Delta T_s}$, the average temperature excursion. The average temperature increase in each branch is derived from its electrical resistance increase. This is accomplished by performing measurements at a range of substrate temperatures. A forth order polynomial is fitted to the resistance-temperature data, which is numerically inverted to obtain the average temperature as a function of the electrical resistance.

In a second step the thermopower is determined in the following manner: The central electrode is heated to create a temperature difference between the center and ends of the suspended sample. The thermopower $S$ is the voltage induced by the Seebeck effect divided by this temperature difference, i.e. $S = -\Delta V/\Delta T$. This means that electric potential and temperature differences between the central segment and the ends have to be measured.

The temperature increase of the central supported segment of the sample is again determined by measuring the increase of its electrical resistance due to the heating current. It is denoted by $\Delta T_{s,max}$, since the maximum temperature increase is expected at the Joule heated central electrode (see Fig. 3b). $\Delta T_{s,max}$ can be inferred from the measured temperature increase averaged over the suspended segments of the sample, $\Delta T_s$, by assuming a linear temperature profile in absence of self heating and modes of heat transfer other than conduction: $\Delta T_{s,max} = 2\Delta T_s$. Any measurable deviation from a linear profile can be avoided by applying small enough currents through the sample during the resistance measurement.

Clearly a prerequisite to the accuracy of this approach is that the sample resistance can be accurately measured while a heating current is applied simultaneously. The feasibility is not obvious since sample and electrode are electrically connected, which means they could interfere. Based on Kirchhoff's current law which is valid in this case of low frequency currents, interferences can be avoided if at least one of the sources has a floating ground, or in other words is isolated from ground. The case of a floating heating current source is depicted in the equivalent circuit of the device, Fig. 1b. Since

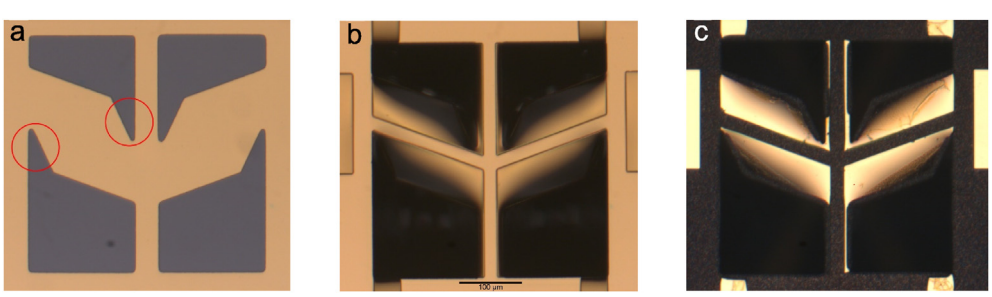


**Fig. 2 – Optical microscope images of the microdevices at different stages of the fabrication process, namely (a) after the first lithography and etching of the exposed metals, two of the notches have been circled, (b) after anisotropic wet etching of the underlying silicon and the second lithography and finally (c) after electroplating into the prepared molds and stripping the photoresist. The final steps are etching of supporting silicon dioxide and exposed metals to obtain free-standing samples.**

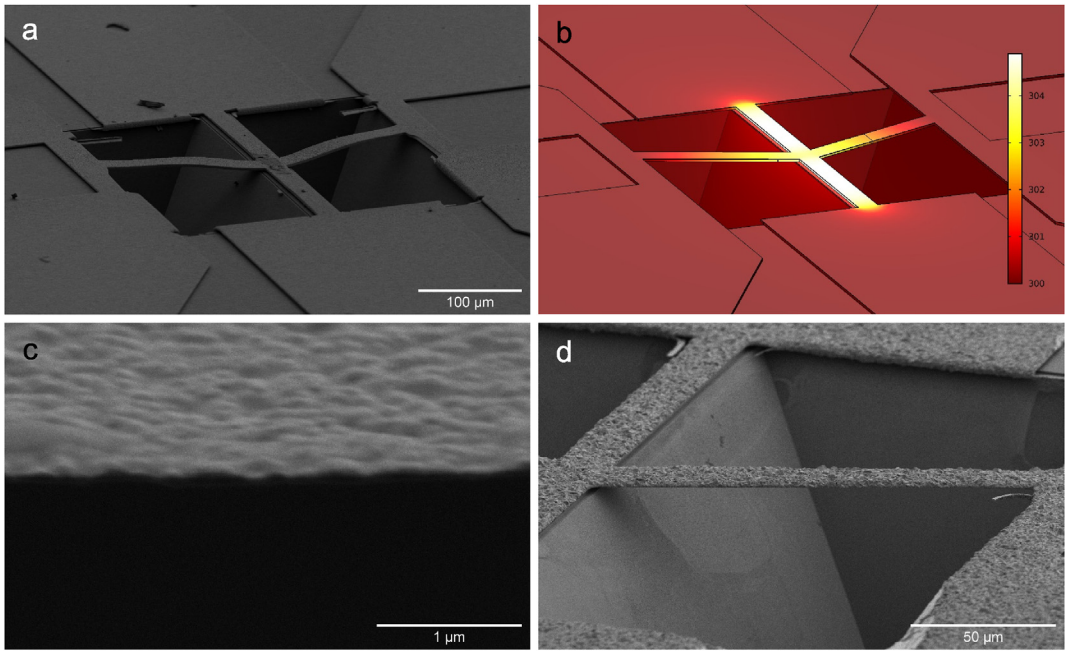


**Fig. 3 – SEM image of a completed microdevice with electrodeposited bismuth telluride. (a) Together with an image of the finite element model (b). The surface temperature in K is indicated by a color map. SEM images of the nickel (c) and bismuth (d) sample are also displayed thermal grease was applied to avoid unwanted temperature gradients between the copper blocks and the sample ends.**

charge accumulation can not occur at low frequencies, the currents flowing out of and into the source $V_h$ must be equal. As no current can be drawn from or flow to ground this implies that $I_{h,1} = I_{h,2}$. Moreover applying Kirchhoff's current law to the node formed by the junction of all four resistors yields $I_{h,1} - I_{h,2} + I_{s,1} - I_{s,2} = I_{s,1} - I_{s,2} = 0$. Therefore in case of a floating ground the currents do not interfere and the resistance of the sample $R_{s,1} + R_{s,2}$ can be determined irrespective of the heating current. This observation holds true for arbitrary values of the four resistances. In general the voltage read by the meter depicted in Fig. 1b is

$$V = R_{s,2}I_s + R_{h,1}I_h - S\Delta T_{s,max}. \quad (1)$$

Here it is assumed that the Seebeck coefficient of the supported central electrode is negligible. It should be noted that generally the contribution due to the Seebeck effect is $(S_{el} - S)\Delta T_{s,max}$, where $S_{el}$ is the Seebeck coefficient of the electrode. $S_{el}$ in turn can be approximated to $S_{el} \approx S_{Au} + (S - S_{Au})\frac{G}{G_{Au}}$ for small $G/G_{Au}$, where $G$ is the electrical conductance of the electrodeposited part of the electrode and $G_{Au}$ that of the underlying gold. This takes account of the electrode being a composite of gold and the deposited material. As the Seebeck coefficient of gold is below 2.2 μV/K in the studied range of temperatures [23,24], $S_{el}$ can be ignored if the conductance of the deposited material is much smaller than the gold's. Particularly when n-type materials are studied, as in the present case, the Seebeck coefficient of the electrode can be close to 0 as the thermopowers of the composites cancel, however the relative nature of the measurement has to be considered especially when materials of low thermopower are studied. There are several ways of extracting from the measured voltage the desired thermovoltage $-S\Delta T_{s,max}$. In the present case the most advantageous is to apply AC heating currents (on the order of 100 kHz). Since the other voltages are applied and measured by National Instruments data acquisition modules at a sampling rate about 2 Hz, voltages due to the AC heating current are averaged out when the frequency of the heating source is sufficiently high.

Isolation from ground of the AC source is ensured by using the secondary current of a transformer powered in our case by a function generator. This has the additional advantages that constant voltage offsets of the source are eliminated and impedance matching allows achieving increased heating currents.

In practice the Seebeck coefficient is measured by performing linear sample current sweeps of small amplitude while simultaneously increasing the alternating heating current amplitude (see Sec. 3.2). The slope of the V-I curves again indicates the sample resistance, since the last two terms in Equation (1), $R_{h,1}I_h - S\Delta T_{s,max}$, are independent of the sample current $I_s$. The offset of the curves is the thermovoltage (the second term in Equation (1), $R_{h,1}I_h$, is averaged out).

### 2.2. *Fabrication*

The fabrication of the microdevices begins with the thermal oxidation of ⟨100⟩ silicon wafers. These were purchased from the Center of MicroNanotechnology, Lausanne. Electron-beam evaporation was then employed to deposit 5 nm Cr/1 μm Au films, using an Alliance-Concept EVA760. Photolithography was applied to pattern the underlying metal films and oxide by

etching, see Fig. 2a. The oxide/metal films then serve as mask for the anisotropic etching of the underlying silicon. A potassium hydroxide solution was chosen as the etchant due to its low toxicity and high ⟨110⟩, ⟨100⟩ selectivity. During this process the metal/oxide layer is partially suspended, namely the areas onto which the sample is subsequently deposited (see Fig. 2b and also 1a). The central segment is still supported after the etching process because its edges are aligned with ⟨110⟩. The notches in the design (see Fig. 2a) have the purpose to facilitate undercutting. The suspended supports of the samples were deliberately designed to be much wider than the sample. This prevents deposition at the edge of the support to be joined with the sample due to overgrowth during electroplating at a later stage. After silicon etching a second lithography is carried out to obtain templates for electroforming. During this process bubble formation due to trapping of air or accumulation of resist in the etch pits had to be avoided.

After carrying out the electrodeposition, the photoresist is stripped and the oxide on the backside of the suspended structures is etched using buffered hydrofluoric acid. Subsequently the exposed metals on the top and backsides are etched, which leaves a sample with two freely suspended branches, concluding the fabrication. Figure 3a is a SEM image of a completed device. All samples were deposited under constant applied potential. In case of $Bi_2Te_3$ the electroplating bath consisted of 10 mM Te (IV), 7.5 mM Bi(III) in 1 M nitric acid as supporting electrolyte [25] and deposition was carried out at 40 mV against sat. Ag/AgCl at room temperature. Bismuth was also deposited from 1 M nitric acid containing 0.1 M Bi(III) [26] and deposition was carried out at −40 mV against sat. Ag/AgCl at room temperature. Finally Ni was deposited from a 1.9 M solution of nickel sulphate at −1 V against sat. Ag/AgCl at room temperature.

In case of $Bi_2Te_3$ a film of thickness 2.05 μm with a root mean square (rms) roughness of about 100 nm was deposited, in case of bismuth 1 ± 0.27 μm and in case of Ni 74 ± 13 nm. Reasons for reducing the thickness of the in particular electrically more conductive Bi and Ni samples are stated in Sec. 3.2.

### 2.3. *Setup and reference sample preparation*

All measurements on the microdevices were carried out in a self-made setup in high vacuum to avoid convective heat transfer. It consists of insulated nichrome wire clamped between two copper plates. The sample holder (consisting of a smaller Cu plate) is mounted on these plates and all electrical leads are clamped between the copper plates and the sample holder. This prevents heat transfer by the wires soldered between the leads and the dies, which becomes important at large substrate to room temperature differences. A platinum resistance thermometer was glued to the substrate holder with thermally conductive epoxy. Additionally a radiation shield surrounding the die was thermally anchored to the copper plates to minimize radiation heat transfer to the wall of the chamber. The substrate temperature is controlled by a PID controller to mK precision.

Apart from numerical studies and comparison to literature the approach was validated by comparison to measurements on reference samples in case of thermopower. These were deposited together with the studied microdevices, i.e. the reference samples were deposited simultaneously in the same electrochemical cell and at the same potential as the microdevices. For the reference samples the substrate consisted of silicon wafers spin coated with a thin film of PMMA. Gold was sputtered onto these as a seed layer. After electrodeposition pieces of glass slides were glued to the deposit using epoxy. As the adhesion between gold and PMMA is much weaker than the adhesion between epoxy and the sample, the samples could be easily mechanically detached from the substrate. Any residual PMMA was removed with acetone and the seed layer was etched using a potassium iodide solution. Measurements of the thermopower of these samples were performed in a self-built setup and also with a commercial device (Linseis LSR-3). The self-built setup consisted of two resistance wires embedded in two copper block. The temperature of each block was determined by platinum resistance thermometers. Bi-directional temperatures gradients were obtained by applying heating currents to each coil separately. Each end of the reference sample was clamped to one of the blocks and the electrical potential difference measured by thin Cu wires (50 μm diameter) soldered to the samples. As all other measurements, the reference measurements were carried out in vacuum and thermal grease was applied to avoid unwanted temperature gradients between the copper blocks and the sample ends.

### 2.4. *Numerical modelling*

Most characterization methods, particularly for microscale samples, are subject to some degree to systematic errors. In this context finite element analysis (FEA) is a useful tool to estimate the significance of these errors. The modelling efforts, using COMSOL Multiphysics 5.5, were based on mimicking as closely as possible the fabricated devices and the measurement process, see Fig. 3b.

The material and dimensional properties were obtained either from the supplier (thickness of wafer and wet thermal oxide), previous measurements (thermoelectric properties and temperature coefficient of resistance of bismuth telluride) and literature (electrical conductivity of gold and specific heat and density of all materials, relevant only for transient studies) or were inferred (thermal conductivity of gold based on the Wiedemann–Franz law). All the material and dimensional properties except for the electrical resistivity of the sample were assumed to be constants. A linear temperature dependence of the electrical resistivity, i.e. $\rho_s(x) = \rho_{s,0}\,(1 + \alpha(T(x) - T_0))$, was assumed, which is reasonable if the temperature excursions are small. Here $\alpha$ is the temperature coefficient of resistance and $\rho_{s,0}$ the resistivity at $T_0$ (i.e. the substrate temperature). The potential difference between the ends of the sample was determined as a function of various applied currents through the sample and positive, null and negative heating currents. The value of the heating current was chosen to generate temperature excursions of the junction between sample and electrode of about 5 K (between 100 and 350 mA in magnitude). Other studied parameters included sample properties and also the thickness of the gold and oxide layers. The applied heating current was adjusted as a function of the latter parameters to maintain the temperature excursion at

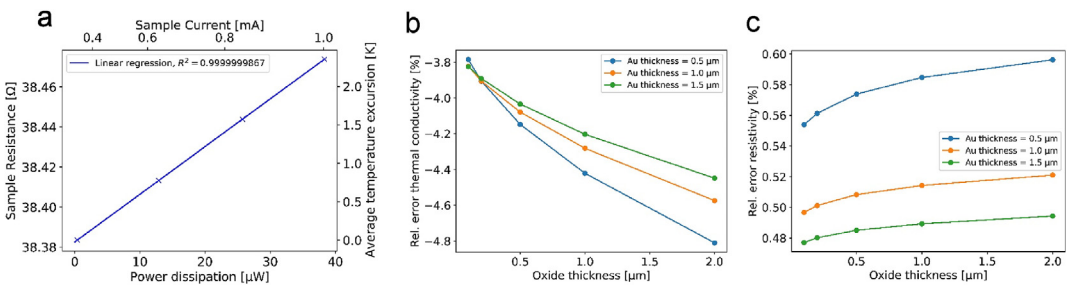


**Fig. 4 – The computed sample resistance as a function of the applied power including the line of best fit (a). From the slope and sample dimensions the thermal conductivity can be obtained, the relative error is plotted as a function of oxide and metal film thickness (b). The relative error of the measured resistivity is displayed again as a function of oxide and metal film thickness (c).**

5 K. Based on the applied currents and the computed voltages the thermoelectric properties of the samples were obtained in the same way as from the measurements, except that means of sweeps performed at positive and negative direct heating currents $I_h$ were computed instead of applying alternating currents. A steady state frequency domain study does not seem feasible since constant currents have to be simultaneously applied and a transient model would significantly increase the computation time.

## 3. Results and discussion

### 3.1. *Numerical modelling*

Figure 4a is an example of a linear regression of the resistance as a function of power, obtained from post-processing the FEA results. Figure 4b displays the deviation of the resulting from the set thermal conductivity (2 $Wm^{-1}K^{-1}$) as a function of metal and oxide film thickness and Fig. 4c shows the deviation of the simulation-based from the set electrical conductivity (150 kS/m). Generally the thickness was set to 2 μm, the thermopower to 80 $\mu VK^{-1}$ and the temperature coefficient to 0.001 $K^{-1}$.

The influence of the relevant parameters on the systematic measurement error is discussed in the following. As expected the error in the electrical conductivity measurement does not significantly depend on the thickness of the metal or oxide film.

The error in the thermal conductivity measurement has a clear increasing trend with increasing oxide thickness and decreasing metal film thickness. Increasing the oxide thickness causes the thermal resistance between the sample and the surrounding substrate to increase and for equal power dissipation this causes the temperature difference between the supports of the sample and the substrate to increase, which is assumed to be negligible. Thinning the metal film decreases its efficiency at conducting heat and therefore this also increases the error.

Figure 5b shows the error in the estimation of $\Delta T$ again as a function of metal and oxide film thickness. Here the temperature difference computed from the resistance increase was compared with the actual difference of the sample temperature close to the edge of the central electrode and the sample temperature at the edge of the pit. These temperatures were chosen in recognition that temperature excursions within supported segments of the sample do not matter as arising potential differences are eliminated by the supporting metal film. It can be observed that the error in the temperature measurements accounts to a large degree for the error of the thermopower measurement (see Fig. 5a). This is even more obvious when variations in the width of the central electrode caused by underetching are ignored, which were accounted for in the presented case. Clearly the error of the temperature decreases with the oxide thickness. The main reason for this is that the heating power has to be increased to maintain the temperature excursion as the oxide film thickness decreases. The increased heat flux into the substrate causes the temperature of the substrate around the sample to increase. For the same reason the error increases with the width of the central bridge. The lower heat flux in case of a narrower bridge leads to a more accurate temperature difference measurement, since the accuracy of this measurement rests on the assumption that the temperature at the ends of the sample does not deviate from that of the heatsink.

It should also be noted that significantly improved accuracy can be achieved by suspending samples over through-holes etched into the Si-chips from the backside, but applying the same measurement method. In this manner, based on both numerical and preliminary experimental results, significantly more accurate measurements (systematic errors smaller than 4%) can be achieved. The reason is that improved thermal isolation between the ends of the sample can be achieved, as through-holes of arbitrary dimension are feasible. Moreover this limits the exposure of the sample to the wet etchants, as the etching processes can be mostly carried out from the backside and also offers direct observation of the sample's underside to detect residual metal.

Apart from studying the influence of design parameters the range of applicability was also investigated by determining measurement errors as a function of the sample properties. The relative errors were studied for a set of thermal and electrical conductivities, see Fig. 6 (the measurement errors were found to have a negligible dependence on the thermopower in the range of 10–210 $\mu VK^{-1}$). All other properties were maintained constant. The thermal conductivity error clearly

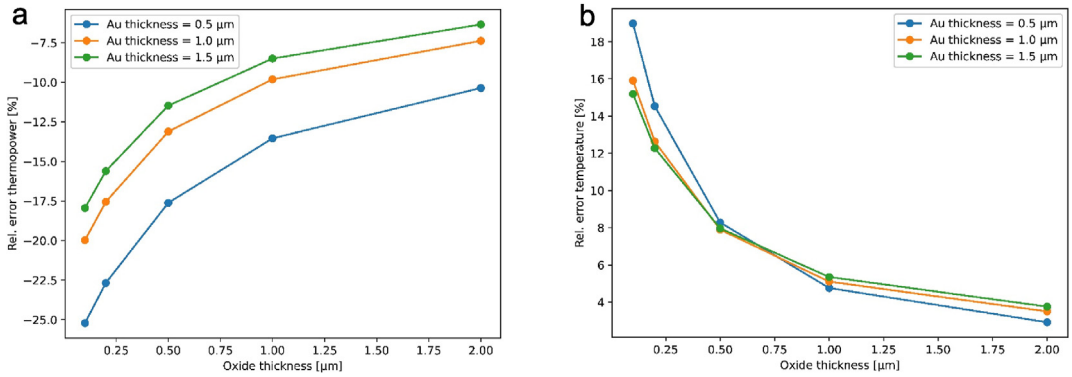


**Fig. 5 – Relative error of the thermopower as a function of metal and oxide film thickness (a). Relative deviation of the determined temperature excursion from the average temperature excursion of the supported segment (b).**

increases with the sample's thermal conductance. More significant is the dependence of the thermopower measurements on the electrical conductance. A main contribution to this is that the thermoelectric properties of supported areas become more heavily weighted by the deposited material instead of the underlying metal. More thermally and electrically conductive samples have to be compensated for by decreasing the film thickness: To maintain the systematic thermopower error below 10% the thermoelectric film's sheet resistance should exceed 1.4 Ω/sq. As the sample's sheet resistance approaches that of the underlying gold (about 0.03 Ω/sq), which means that $G/G_{Au}$ approaches 1, an expected significant underestimation of the thermopower occurs.

To assess their impact on the results, thermal and electrical contact resistances were included. For the thermal interface resistance between the thermoelectric and gold $2 \times 10^{-6}$ $m^2KW^{-1}$ were chosen based on the measurement by the photoacoustic method [27] on an interface obtained by electroplating bismuth telluride on nickel. The contact resistance between gold and silicon oxide was determined by oxide layer thickness dependent measurements to be less than $10^{-8}$ $m^2KW^{-1}$ [28]. The thermal interface resistance between oxide and underlying silicon was ignored as a value less than $10^{-9}$ $m^2KW^{-1}$ is expected [29]. Finally based on [30] 5 $\mu\Omega cm^2$ can be considered an upper bound for the electrical contact resistance. With these values the error of the thermal conductivity measurement increases to 5%, while the thermopower error decreases. These results indicates that contact resistances should be taken into account, for instance by performing sample length dependent measurements, but are expected to have limited impact.

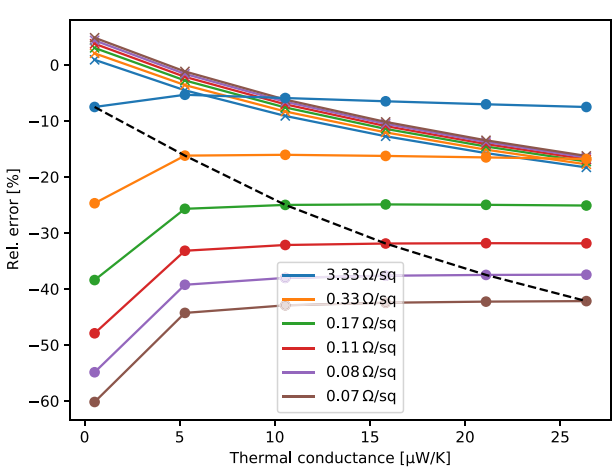


**Fig. 6 – Relative error of the thermal conductivity measurement (crosses) and the thermopower measurement (circles) as a function of the sample's thermal conductance and sheet resistance. The dashed black curve connects points for which thermal and electrical conductance are coupled and thus provides an estimate of the film thickness dependence of the error.**

In conclusion of the numerical studies one can observe that the thickness of the metal film should be maximized since it decreases the systematic error in the measurement of all thermoelectric properties. The thickness of the oxide layer correlates with an increase of the thermal conductivity measurement error, however also with a decrease of the thermopower measurement error. The latter dependence is more significant. Also the error on the thermopower contributes twice as much to the overall error on the figure of merit, since it depends on the square of the thermopower. Therefore a thermal oxide and gold film thickness of 1 μm was chosen as a trade-off.

### 3.2. *Measurements*

As mentioned the electrical sample resistance is determined from sample current sweeps of peak values below 100 μA resulting (for typical sample resistances) in heating power less than 1 μW and therefore temperature excursions on the order of only 1 mK, which is negligible. The thermal conductance is obtained from the static resistance as a function of power. The sample dimensions are obtained from SEM micrographs and based on these thermal and electrical conductivity can be derived, as displayed in Fig. 7a and b. The uncertainty in the sample dimensions is the main contribution to the error bars. The Seebeck coefficient is determined by measuring the sample resistance while applying alternating heating currents of increasing amplitude. The slope and offset of the obtained

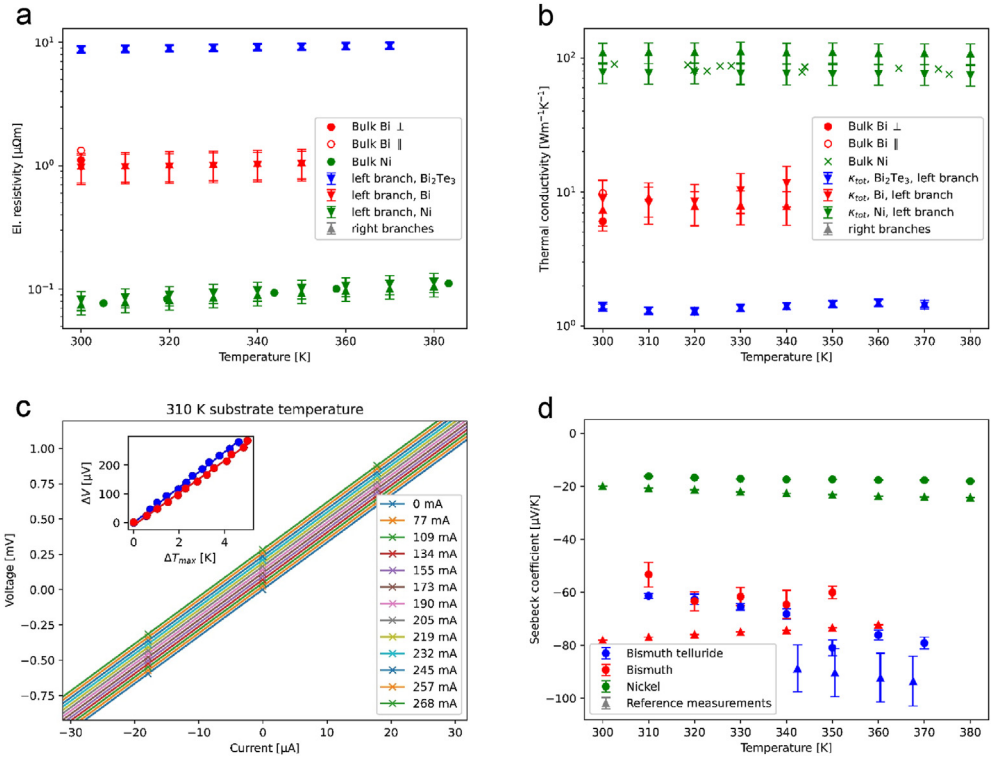


**Fig. 7 – (a) Resistivity of the two branches of the Bi, Ni and $Bi_2Te_3$ samples, measured by the pseudo-4-probe method. Bulk measurements are taken from [32] in case of Bi and [33] in case of Ni. (b) The thermal conductivity is displayed for both branches and all three samples. Reference values are from the same sources as for (a). (c) The voltage drop along the right sample branch is plotted against the current through the sample for increasing AC heating currents (approximate peak values). The increasing offset is equal to the thermovoltage, while the resistance is derived from the slope (the increase of the slope is too small to be noticed by bare eye). The inset is a representative example of a thermovoltage–temperature curve for both branches of the sample, which is the result of analyzing the family of curves. (d) Comparison of the measured thermopower with reference measurements on the Bi, Ni and $Bi_2Te_3$ samples. For the sake of clarity the thermopower is in each case displayed for one of the two suspended branches only. The reference measurements were obtained with a Linseis LSR-3 device in case of bismuth telluride and a self-built setup for the other samples.**

V-I curves indeed increase with the heating current, as illustrated by Fig. 7c, indicating the increasing resistance/temperature and the thermovoltage respectively. Since the thermovoltage measurements are most prone to systematic errors based on the numerical modelling, they are compared to measurements on reference samples (Fig. 7d) that were in each case deposited together with the microdevices and released from the conducting substrate by a lift-off process and etching. In accordance with the numerical modelling the thermopower is always underestimated, however consistently by about 20%, which is much greater than the expected deviation. Some contributing factors can be identified. Firstly, it was determined by 4 point probe measurements that the resistivity of the underlying gold film is 32% greater than assumed in the finite element model, and it was demonstrated that increased errors can be expected in this case (cf. Figure 5a). Secondly as mentioned above abnormal undercutting occurs, likely due to galvanic coupling between gold and chromium [31], which intensifies the width variation along the central electrode. This can lead to temperature gradients close to the junction and therefore an overestimation of the temperature difference. As mentioned above, based on numerical studies and also preliminary experimental results significant improvements can be expected by fabricating devices over through-holes in the substrate, but employing the same measurement method.

The reference measurement on $Bi_2Te_3$ was carried out by a Linseis LSR-3, the others were performed on a setup described above. The results of electrical and thermal conductivity measurements are compared to values from literature, at least in case of the pure metal samples. The significantly greater uncertainty in case of the Ni and Bi samples is caused by the uncertainty in the sample dimensions: the bismuth sample has greater relative roughness and this is also true for the nickel sample because less than 100 nm of nickel were deposited. The reason for this choice is that nickel has a significantly greater electrical conductivity and therefore would have an accordingly greater impact on the Seebeck coefficient measurement. Additionally the higher conductivity implies that the sample current would need to be increased beyond hardware imposed limits to achieve sufficient temperature excursions, if the thickness is not reduced.

Nonetheless the electrical and thermal conductivities are in good agreement to values from literature. Generally also measurements on both branches are in good agreement. The exception is the nickel sample caused by a tear in the left sample and residual material on the right branch.

The results on bismuth telluride were further analyzed. These samples (reference samples and microdevices) were annealed prior to the thermoelectric characterization, as in case of $Bi_2Te_3$ electrical resistance drift was observed, particularly at higher temperatures. The drift at constant temperature occurs at usually increasing rates of about 0.2 Ω/h or 3.5‰/h. Further investigation is required, but stabilization could be achieved by annealing at 215 °C for 2 h in air. Higher temperatures were avoided to prevent significant diffusion of gold into the sample [34]. This had no measurable effect on the composition, determined by energy dispersive X-ray spectroscopy to be 41 at. % bismuth, but induced grain growth (see Supporting Information (SI)). The lattice contribution of the thermal conductivity $\kappa_l$ is isolated by subtracting the charge carrier contribution, which is derived from the Wiedemann–Franz law, i.e. $\kappa_l = \kappa_{tot} - L\sigma T$. The Sommerfeld value for degenerate conductors is used as the Lorenz number, i.e. $2.44 \times 10^{-8}$ $W\Omega K^{-2}$. It is well known that narrow-bandgap semiconductors such as $Bi_2Te_3$ can exhibit bipolar conduction [35,36] and therefore significantly enhanced Lorenz numbers in the transition region, however the electrical conductivity is nearly an order of magnitude higher than one would expect in this case [18,37], which means that this contribution can be ignored at least at low temperatures. After subtracting the charge carrier contribution the obtained lattice component does not monotonically decrease with temperature against expectation, indicating that the contribution due to intrinsic carriers could become significant at the higher substrate temperatures (see SI).

At room temperature the value obtained for the lattice thermal conductivity is 0.5 $Wm^{-1}K^{-1}$, which falls short of the values of 1.5 and 0.7 $Wm^{-1}K^{-1}$ reported for transport along and across the basal plane of single crystals respectively [38–41]. To a large degree this can be attributed to scattering at grain boundaries. It was determined by X-ray diffraction (XRD) that the grain size is on the order of 100 nm and that grains have a weakly preferred ⟨101⟩ and ⟨100⟩ orientation (SI). Although the grain size exceeds the phonon mean free path by orders of magnitude one can expect a decrease of the lattice thermal conductivity by nearly 50% at least along the trigonal direction [41,42] based on modelling for this case. The experimental results are in good agreement with those of Takashiri et al. who studied the lattice thermal conductivity of flash evaporated nanocrystalline $Bi_2Te_3$ as a function of grain size. The thermal conductivity was measured using a differential $3\omega$ method in this study and various grain sizes were obtained by annealing at 150 and 250 °C. After annealing at 250 °C at a grain size of 60 nm the authors find a lattice thermal conductivity of 0.4 $Wm^{-1}K^{-1}$. A value of 0.5 $Wm^{-1}K^{-1}$ at grain sizes between 100 and 300 nm follows well the trend observed by the authors.

The observed significant deviation from measurements on bulk samples in case of $Bi_2Te_3$ raises the question why similar deviations were not observed in case of the studied Ni and Bi samples. Different reasons apply. In case of nickel the lattice contribution comprises only a few percent of the total thermal conductivity, particularly around room temperature [33]. Changes in the lattice contribution are therefore difficult to observe and boundary scattering typically affects phonons before charge carriers as the length scale is decreased. In case of the bismuth sample the situation is different, charge carriers and phonons contribute approximately equally to the thermal conductance at room temperature. However the grain sizes in this sample are at least one order of magnitude greater compared to the other studied samples, i.e. greater than 1 μm. This was not determined by XRD but the plating conditions are the same as in Sandnes et al. [26], who report grains of this size, and this is also consistent with the coarse grained appearance of this sample under scanning electron microscopy (SEM) compared to the others. In general the samples appear to be compact and uniform, which is consistent with the typically good agreement between measurements on either branches.

## 4. Conclusion

Micro-bridge devices for the complete in-plane thermoelectric characterization of deposited films were developed, fabricated and investigated. Compared to competing comprehensive thermoelectric characterization methods for deposited films, all based on suspended microdevices, the developed approach is distinguished by a simple fabrication process and accuracy for a wide range of sample properties. The validity of the method was first verified by mimicking the experiments by finite element analysis. The underlying analytical assumptions were demonstrated to hold true as a wide range of assumed material properties could be recovered accurately numerically. In general good accuracy can be achieved if the sample's sheet resistance exceeds about 1.4 Ω/sq to avoid excessive errors in the thermopower measurement.

Secondly the method was verified experimentally by comparing to measurements of the thermopower on simultaneously deposited reference samples as well as results from literature. In accordance with finite element analysis we find that the measurements of thermal and electrical conductivity are in excellent agreement with literature and can be considered accurate. Deviations from bulk measurements were only observed in case of the nanocrystalline $Bi_2Te_3$ sample, which displayed a lower lattice thermal conductivity than the bulk. This was attributed to enhanced grain boundary scattering of phonons in agreement with previous results. In conclusion significant systematic errors on the electrical resistivity and the thermal conductivity could be excluded in case of all studied materials.

The thermopower is expected to be most prone to systematic errors based on the numerical modelling, however a greater than expected deviation of 20% from the reference measurements was observed in all cases. This is likely mainly caused by a greater than expected resistivity of the supporting gold film and abnormal undercutting while etching gold due to galvanic effects. Design changes that improve the accuracy were discussed and are currently under investigation. The developed method represents a simpler and widely applicable approach for the complete thermoelectric characterization of deposited films.

## Declaration of Competing Interest

The authors declare that they have no known competing financial interests or personal relationships that could have appeared to influence the work reported in this paper.

## Acknowledgements

D. O. acknowledges funding by the Swiss National Science Foundation (project no. 200021E-175703). This work was also supported by the French National Research Agency (grant no. ANR-17-CE05-0027). We thank Dr. Johann Michler for fruitful discussions.

## Appendix A. Supplementary data

Supplementary data to this article can be found online at https://doi.org/10.1016/j.jmrt.2021.08.109.

REFERENCES

[1] Gayner C, Kar KK. Recent advances in thermoelectric materials. Prog Mater Sci 2016;83:330–82. https://doi.org/10.1016/j.pmatsci.2016.07.002.
[2] Martín-González M, Caballero-Calero O, Díaz-Chao P. Nanoengineering thermoelectrics for 21st century: energy harvesting and other trends in the field. Renew Sustain Energy Rev 2013;24:288–305.
[3] Kim J, Bahk JH, Hwang J, Kim H, Park H, Kim W. Thermoelectricity in semiconductor nanowires. Phys Status Solidi Rapid Res Lett 2013;7(10):767–80. https://doi.org/10.1002/pssr.201307239.
[4] Wu M, Ramírez SA, Shafahian E, Guo L, Glorieux C, Binnemans K, et al. Electrodeposition of bismuth telluride thin films containing silica nanoparticles for thermoelectric applications. Electrochim Acta 2017;253:554–62. https://doi.org/10.1016/j.electacta.2017.09.012.
[5] Burton MR, Richardson SJ, Staniec PA, Terrill NJ, Elliott JM, Squires AM, et al. A novel route to nanostructured bismuth telluride films by electrodeposition. Electrochem Commun 2017;76:71–4. https://doi.org/10.1016/j.elecom. 2017.02.004.
[6] Harman TC, Walsh MP, Laforge BE, Turner GW. Nanostructured thermoelectric materials. J Electron Mater 2005;34(5):L19. https://doi.org/10.1007/s11664-005-0083-8.
[7] Harman TC, Taylor PJ, Spears DL, Walsh MP. Thermoelectric quantum-dot superlattices with high ZT T.C. J Electron Mater 2000;29(1):1–4. https://doi.org/10.1007/s11664-000-0117-1.
[8] Winkler M, Liu X, Schürmann U, König JD, Kienle L, Bensch W, et al. Current status in fabrication, structural and transport property characterization, and theoretical understanding of Bi2Te3/Sb2Te3 superlattice systems. Zeitschrift fur Anorg und Allg Chemie 2012;638(15):2441–54. https://doi.org/10.1002/zaac. 201200305.
[9] Venkatasubramanian R, Siivola E, Colpitts T, O'Quinn B. Thin-film thermoelectric devices with high room-temperature figures of merit. Nature 2001;413(6856):597–602. https://doi.org/10.1038/35098012.
[10] Manzano CV, Abad B, Muñoz Rojo M, Koh YR, Hodson SL, Lopez Martinez AM, et al. Anisotropic effects on the thermoelectric properties of highly oriented electrodeposited Bi2Te3 films. Sci Rep 2016;6(1):19129. http://www.nature.com/articles/srep19129.
[11] Cahill DG. Thermal conductivity measurement from 30 to 750 K: the 3$\omega$ method. Rev Sci Instrum 1990;61(2):802–8. https://doi.org/10.1063/1.1141498.
[12] Nomura M, Kage Y, Müller D, Moser D, Paul O. Electrical and thermal properties of polycrystalline Si thin films with phononic crystal nanopatterning for thermoelectric applications. Appl Phys Lett 2015;106(22). https://doi.org/10.1063/1.4922198.
[13] Hu H, Wang X, Xu X. Generalized theory of the photoacoustic effect in a multilayer material. J Appl Phys 1999;86(7):3953–8. https://doi.org/10.1063/1.371313.
[14] Abad B, Borca-Tasciuc DA, Martin-Gonzalez MS. Non-contact methods for thermal properties measurement. Renew Sustain Energy Rev 2017;76(April):1348–70. https://doi.org/10.1016/j.rser.2017.03.027.
[15] Rojo MM, Manzano CV, Granados D, Osorio MR, Borca-Tasciuc T, Martín-González M. High electrical conductivity in out of plane direction of electrodeposited Bi2Te3 films. AIP Adv 2015;5(8). https://doi.org/10.1063/1.4928863.
[16] Kim P, Shi L, Majumdar A, McEuen PL. Thermal transport measurements of individual multiwalled nanotubes. Phys Rev Lett 2001;87(21). https://doi.org/10.1103/PhysRevLett.87.215502. 215502–1–215502–4.
[17] Mavrokefalos A, Pettes MT, Zhou F, Shi L. Four-probe measurements of the in-plane thermoelectric properties of nanofilms. Rev Sci Instrum 2007;78(3):1–6. https://doi.org/10.1063/1.2712894.
[18] Mavrokefalos A, Moore AL, Pettes MT, Shi L, Wang W, Li X. Thermoelectric and structural characterizations of individual electrodeposited bismuth telluride nanowires. J Appl Phys 2009;105(10). https://doi.org/10.1063/1.3133145.
[19] Seol JH, Moore AL, Shi L, Jo I, Yao Z. Thermal conductivity measurement of graphene exfoliated on silicon dioxide. J Heat Tran 2011;133(2):022403. http://link.aip.org/link/JHTRAO/v133/i2/p022403/s1{&}Agg=doi.
[20] Barati V, Garcia Fernandez J, Geishendorf K, Lu Schnatmann, Lammel M, Kunzmann A, et al. Thermoelectric characterization platform for electrochemically deposited materials. Adv Electr Mater 2020;1901288:1–8. https://doi.org/10.1002/aelm.201901288.
[21] Völklein F, Reith H, Cornelius TW, Rauber M, Neumann R. The experimental investigation of thermal conductivity and the Wiedemann-Franz law for single metallic nanowires. Nanotechnology 2009;20(32). 0–8, http://stacks.iop.org/Nano/20/325706.
[22] Karg S, Mensch P, Gotsmann B, Schmid H, Kanungo PD, Ghoneim H, et al. Measurement of thermoelectric properties of single semiconductor nanowires. J Electron Mater 2013;42(7):2409–14. https://doi.org/10.1007/s11664-012-2409-7.
[23] Cusack N, Kendall P. The absolute scale of thermoelectric power at high temperature. Proc Phys Soc 1958;72(5):898–901. https://doi.org/10.1088/0370-1328/72/5/429.
[24] Laubitz MJ. Transport properties of pure metals at high temperatures. II. Silver and gold. Can J Phys 1969;47(23):2633–44. https://doi.org/10.1139/p69-322.
[25] Martín-González MS, Prieto AL, Gronsky R, Sands T, Stacy AM. Insights into the electrodeposition of Bi2Te3. J Electrochem Soc 2002;149(11):C546. http://jes.ecsdl.org/cgi/doi/10.1149/1.1509459.
[26] Sandnes E, Williams ME, Bertocci U, Vaudin MD, Stafford GR. Electrodeposition of bismuth from nitric acid electrolyte. Electrochim Acta 2007;52(21):6221–8. https://doi.org/10.1016/j.electacta.2007.04.002.
[27] Mishra H, Cola BA, Rawat V, Amama PB, Biswas KG, Xu X, et al. Thermomechanical and thermal contact characteristics of bismuth telluride films electrodeposited on carbon nanotube arrays. Adv Mater 2009;21(42):4280–3. https://doi.org/10.1002/adma.200803705.

[28] Käding OW, Skurk H, Goodson KE. Thermal conduction in metallized silicon-dioxide layers on silicon. Appl Phys Lett 1994;65(13):1629–31. https://doi.org/10.1063/1.112933.
[29] Gu H, Wang J, Wei X, Wang H, Li Z. Thermal conductivity and interfacial thermal resistance in the heterostructure of silicon/amorphous silicon dioxide: the strain and temperature effect. Nanotechnology 2020;31(50). https://doi.org/10.1088/1361-6528/abb504. 0–12.
[30] Sharma PA, Brumbach M, Adams DP, Ihlefeld JF, Lima-Sharma AL, Chou S, et al. Electrical contact uniformity and surface oxidation of ternary chalcogenide alloys. AIP Adv 2019;9(1). https://doi.org/10.1063/1.5081818.
[31] Green TA. Gold etching for microfabrication. Gold Bull 2014;47(3):205–16. https://doi.org/10.1007/s13404-014-0143-z.
[32] Gallo CF, Chandrasekhar BS, Sutter PH. Transport properties of bismuth single crystals. J Appl Phys 1963;34(1):144–52. https://doi.org/10.1063/1.1729056.
[33] Powell RW, Tye RP, Hickman MJ. The thermal conductivity of nickel. Int J Heat Mass Tran 1965;8(5):679–88. https://doi.org/10.1016/0017-9310(65) 90017-7.
[34] Shaughnessy MC, Bartelt NC, Zimmerman JA, Sugar JD. Energetics and diffusion of gold in bismuth telluride-based thermoelectric compounds. J Appl Phys 2014;115(6).
[35] Goldsmid HJ. Introduction to thermoelectricity. 2010. https://doi.org/10.1007/978-3-642-00716-3.
[36] Kaibe H, Tanaka Y, Sakata M, Nishida I. Anisotropic galvanomagnetic and thermoelectric properties of n-type Bi2Te3 single crystal with the composition of a useful thermoelectric cooling material. J Phys Chem Solid 1989;50(9):945–50.
[37] Pettes MT, Maassen J, Jo I, Lundstrom MS, Shi L. Effects of surface band bending and scattering on thermoelectric transport in suspended bismuth telluride nanoplates. Nano Lett 2013;13(11):5316–22. https://doi.org/10.1021/nl402828s.
[38] Goldsmid HJ. The thermal conductivity of bismuth telluride. Proc Phys Soc B 1956;69(2):203–9. https://doi.org/10.1088/0370-1301/69/2/310.
[39] Goldsmid HJ. Recent studies of bismuth telluride and its alloys. J Appl Phys 1961;32(10):2198–202. https://doi.org/10.1063/1.1777042.
[40] Satterthwaite CB, Ure RW. Electrical and thermal properties of Bi2Te3. Phys Rev 1957;108(5):1164–70. https://doi.org/10.1103/PhysRev.108.1164.
[41] Takashiri M, Miyazaki K, Tanaka S, Kurosaki J, Nagai D, Tsukamoto H. Effect of grain size on thermoelectric properties of n -type nanocrystalline bismuth-telluride based thin films. J Appl Phys 2008;104(8). https://doi.org/10.1063/1.2990774.
[42] Al-Alam P, Pernot G, Isaiev M, Lacroix D, De Vos M, Stein N, et al. Lattice thermal conductivity of Bi2Te3 and SnSe using Debye-Callaway and Monte Carlo phonon transport modeling: application to nanofilms and nanowires. Phys Rev B 2019;100(11):1–16. https://doi.org/10.1103/PhysRevB.100.115304.